Manufacturing Rev. **12**, 7 (2025)

https://doi.org/10.1051/mfreview/2025002

**Manufacturing Review**
Available online at:
https://mfr.edp-open.org

ORIGINAL ARTICLE OPEN ACCESS

# Laser marking method for nonferrous metal casting ingots based on improved RANSAC algorithm

Rui Zheng*

Railway Locomotive School, Jilin Railway Technology College, Jilin 132001, China

Received: 21 October 2024 / Accepted: 13 February 2025

**Abstract.** Non ferrous metal casting ingots must carry relevant production information, usually using manual pasting of copper coated paper, manual lifting of spray code, and pneumatic marking methods. These methods have a low degree of automation and severe material waste. To this end, genetic algorithm (GA) is used to guide sampling of random sample consensus algorithm (RANSAC) based on probability, and the two are combined for simulation to optimize the shortcomings of RANSAC algorithm in random sampling. On the ground of the optimized RANSAC to fit the plane equation, the normal vector of the plane is calculated, and the angle between the coordinate axis and the normal vector in the pendulum coordinate system is determined through the normal vector, enabling automatic alignment and vertical focusing functions to be achieved. Finally, based on the actual situation, the marking position is determined using set relationships to achieve motion control of mechanical functions. A laser marking method for non-ferrous metal casting ingots based on the improved RANSAC algorithm was designed. Through experimental analysis, it was found that the average F1 value of the method is 96.42, the average accuracy is 98.24%, the RMSE is 0.236, and the running time is 18.40 seconds. The F1 value represents the combined performance of the model's accuracy and recall rate when dealing with the marking task. Combined with the above results, it can be seen that the research and design method can efficiently and accurately laser marking metal casting ingot, and improve production efficiency.

**Keywords:** Random sample consistency algorithm / genetic algorithm / laser marking / plane equation fitting

## 1 Introduction

Non ferrous metals play a crucial role in various technological industries in today's society and occur an essential position in developing the national economy. Automated production lines have become a trend in industrial development, and the mechanical positioning method using a fixed focal length structure with mechanical bonding is subject to excessive interference and difficult to adapt to actual needs. When the stacking of casting ingots is transmitted on the production line, the posture of the stacking of casting ingots is uncertain, and the mechanical structure with fixed focal length accumulates over time, resulting in greater errors caused by wear and deterioration of the marking effect [1]. The development of non-contact automatic alignment marking equipment is necessary and urgent. Laser marking has advantages such as stability, high efficiency, and long retention time of marking results [2]. When applied to laser marking in many industries, and in the non-ferrous metal production industry, it is necessary to develop laser marking equipment for stacking non-ferrous metal casting ingots [3,4]. In accordance with a cluster of sample datasets including abnormal data, RANSAC calculates the mathematical model parameters for obtaining valid sample data, which is widely adopted in plane fitting [5]. To this end, the RANSAC is utilized to fit the equation of the metal casting ingot plane, find the closest plane, and remove the noise on the surface of the metal ingot itself. During the process, it was found that the RANSAC algorithm still has certain limitations and poor training performance. Therefore, the GA algorithm was used to optimize it. Perform digital alignment based on the fitted plane equation to improve marking accuracy. Based on this research, a laser marking method for non-ferrous metal casting ingots was designed based on the improved RANSAC algorithm. Intended to provide technical support for the production of metal products and improve product production efficiency.

## 2 Related works

During the laser marking process, the computer uses a laser marking control card to control the laser switch and control the laser beam to move along a predetermined trajectory.

* e-mail: rui_zheng987@163.com

Finally, the corresponding pattern is marked on the surface of the marked object as required. Li et al. proposed a simple, customizable, and low-cost method for developing flexible pressure sensors with high sensitivity and wide linear range. A new layered microstructure was constructed using laser marking technology and a high-performance flexible pressure sensor was implemented [6]. Pandey et al. studied the influences in process parameters, e.g. laser power, pulse frequency, scanning speed, and duty cycle on the intensity, circularity, and other responses of laser marking. Single pass laser marking is performed by scanning a fiber laser without auxiliary air pressure. It was found that choosing a 30% duty cycle and a scanning speed of 5 mm/s can achieve better response [7]. Korakana et al. used a solid-state laser beam to label and analyze the effect of laser etching parameters on the corrosion resistance and surface roughness of marine grade 316 stainless steel using a laser annealing process. Analysis shows that the scanning speed of the laser beam is the biggest factor affecting operation [8]. Rasskazchikov et al. investigated the effect of laser processing parameters on the formation of color gamut in the laser beam influence zone on metal surfaces to optimize the laser marking process. The main drawback of limiting the wider use of laser color marking methods is the lack of predictability in the resulting color processing, as found in experiments [9]. Cucerca et al. formulated a powerful solution to the problem of color gamut exploration that is disproportionate to the high-dimensional design space of laser marking. This exploration formula was transformed into a search for Pareto optimal solutions for multi-objective optimization. Evolutionary algorithms are used to solve and ultimately label high-quality panchromatic images using a set of different colors explored [10]. Eyahanyo et al. successfully labeled apples on horticultural products using a Synrad48-5 CO2 laser at low energy levels [11]. Drobnitzky et al. addressed the issue of the use of geometrically distorted MR images in radiation therapy plans that may affect dosimetry. A new phantom based laser labeling workflow has been proposed for visual evaluation of geometric image distortion in magnetic resonance guided radiotherapy [12].

The Random Sample Consistency Algorithm (RANSAC) obtains the mathematical model parameters of the data built on relevant sample datasets to acquire effective sample data. Gönülta et al. applied the RANSAC algorithm to roof plane recognition using aerial photogrammetric data and LiDAR data. And compared with the laser ranging and detection (LIDAR) algorithm, it was found that the RANSAC algorithm performs better [13]. Cao et al. proposed a new optimal time selection method grounded on RANSAC technology. It can precisely extract the ship centerline in the upper structure and low signal-to-noise ratio of the ship [14]. Bai et al. found that the traditional RANSAC algorithm is unreliable in localization results due to the fact that the choice of thresholds rests with prior knowledge. To perfect the algorithm's universality indoor, an advanced RANSAC in line with adaptive threshold is proposed [15]. Hossein Nejad et al. raised a new four step image stitching way to solve the problem of excessive and time-consuming repetitive key points in the SIFT algorithm. Firstly, redundant key point elimination SIDT (RKEM SIFT) algorithm is utilized to recognize key points in reference and sensing images. The embedding process is improved. Finally, the RANSAC is performed to make sure the adaptive threshold to eliminate mismatch and optimize image stitching [16]. Zhang et al. raised an improved outlier way grounded on RANSAC algorithm to find the correct matching result of the optimal distribution. Integrate the connection point optimization spatial formulation way adopting stratified random sampling (SRS) into the RANSAC framework. This is for filtering out mismatched features generated by the SIFT algorithm [17]. Singh et al. used terrestrial laser scanner (TLS) to retrieve numerical parameters and provide point-cloud data for exact evaluation of forest biomass. Then they carried out the RANSAC to speculate the basic information of the forest [18]. Li et al. proposed a flexible point-cloud matching method in line with correspondence, which evaluates scale and translation parameters through the RANSAC algorithm [19]. Afsal et al. suggested a hybrid RANSAC and M-estimation sample consistency method (MSAC) for stable optimization of camera videos. The matched point pairs are fitted into the affine transformation model to estimate the inter frame motion [20].

From the above literature, the RANSAC is widely taken use in visual image processing. However, in practical applications, the laser marking technology for non-ferrous metal casting ingots still faces significant difficulties. Therefore, a non-contact laser marking method for non-ferrous metal casting ingots was developed using the improved RANSAC algorithm. Realize high-definition and effective surface marking.

## 3 Design of laser marking method for non-ferrous metal casting ingots based on improved Ransac algorithm

### 3.1 GA-RANSAC based fitting of the plane equation of the marked surface

When laser marking the surface of non-ferrous metal casting ingots, the laser marking lens must be able to maintain accurate vertical focus on the surface of the casting ingot. Thus, it is needful to build a plane equation for the marked surface of the casting ingot, and calculate the corresponding rotation angle or displacement of each axis based on the normal vector to achieve automatic alignment. When fitting the plane equation on the surface of non-ferrous metal casting ingots, the presence of noise on it can lead to deviation in the results of plane fitting. If the wrong matching equation is used for marking, it will result in the overall unclear or incomplete marking content. Therefore, this study proposes an improved RANSAC. Using GA to optimize the random sampling process of the algorithm and improve the efficiency of the algorithm, the selection of the marking position of the metal casting ingot is generally flat on the side, and there is generally no phenomenon of stress concentration.

The noise is related to the common defects in the ingot. First, segregation results in an uneven distribution of the material's composition, which is recognized as a noise point

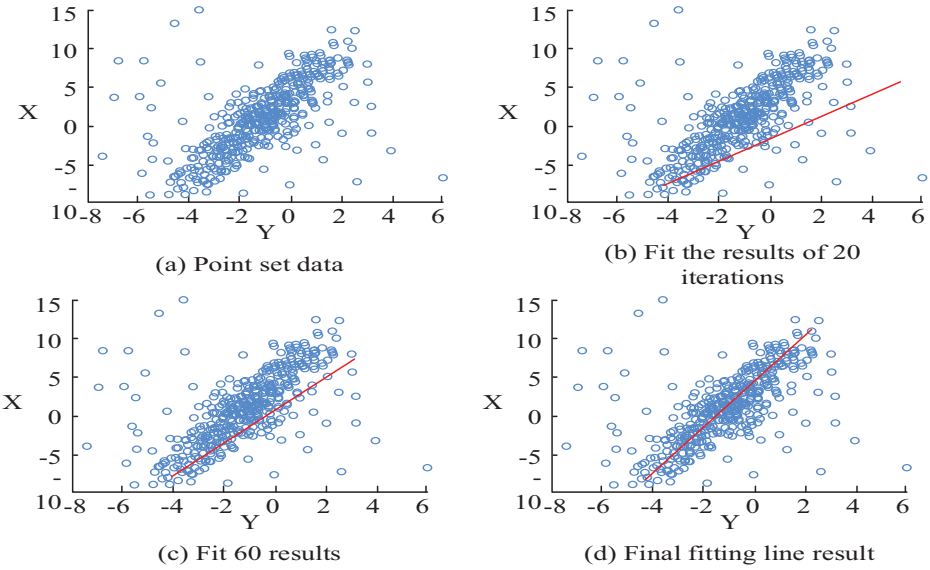


**Fig. 1.** Schematic diagram of using RANSAC algorithm for line fitting of scattered points.

during laser scanning, affecting the accuracy of the plane fit. Secondly, shrinkage holes and cracks can create uneven areas on the ingot surface, which have different reflection characteristics than the surrounding flat surface and are also considered noise. Pores form tiny voids on the surface, and the laser reflection at these locations is abnormal, further increasing the noise data. In addition, the oxidation layer on the ingot surface, residual casting sand and machining marks will also cause interference to the laser reflection signal and form noise. These noise points will be incorrectly included in the calculation during the plane fitting process, resulting in a deviation of the fitted equation. Common defects in metal casting ingots include segregation, shrinkage, cracks, and pores. The main factors that have a significant impact on obtaining surface data of metal casting ingots are segregation nodules and cracks. The biggest impact of segregation on marking is the generation of noise, which must be removed in the algorithm. RANSAC uses an iterative method to estimate mathematical models through a large amount of measurement data, which needs to include interior point data, as well as exterior point data. Outer points are noise points. Firstly, perform line fitting on scattered data, randomly select two points from all point data in the point set, and calculate a set of data containing slope and intercept based on these two points. According to actual requirements, set a threshold in advance to calculate the distance from all points in the rest of points to the line. If the distance is less than the threshold, then this point is an inner point, otherwise it is an outer point.

The study begins by measuring a large sample size of data to determine a reasonable range of distribution that covers most normal data points. Considering the diversity and complexity of defects on the ingot surface, this study uses convolutional neural network to gradually adjust the threshold by training its automatic learning, observe its influence on the plane fitting effect, and finally determine an optimal threshold that can effectively remove noise points without too much misjudgment of normal data points. The final threshold was determined to be 0.5 mm. Repeat the above process continuously until a result that matches the proportion of interior points occurs or the max iteration number is reached to end the iteration. The fitting results before and after the RANSAC algorithm line fitting iteration are shown in Figure 1.

The rise in the iteration number of the RANSAC results in a significant increase in the computation time. The uptime of the algorithm is calculated as in equation (1).

$$T = M(t_s + t_c) + MNt. \tag{1}$$

In equation (1), $M$ is the iterations, $t_s$ is the time to randomly select data from the original data that fit the calculated mathematical model, $t_c$ is the time to calculate the mathematical model based on the sampled data, $N$ is the amount of data to be tested after the mathematical model is calculated, and $t$ is the testing time for each data. In order to obtain better planar equations, the algorithm requires a large increase in the number of extractions $M$, which is not very efficient for training. For this reason, the study optimizes it using GA algorithm, which is an algorithmic model derived from evolutionary theory and genetics to calculate the global optimal solution. The GA algorithm consists of three major parts: population coding and decoding, individual fitness evaluation and genetic operations. It has a good global optimality seeking ability and is able to efficiently upgrade the convergence speed of RANSAC algorithm. The algorithm flow is shown in Figure 2.

Firstly, the point cloud data are coded and formed into index chromosomes using 10 sets of 3D point cloud data indexes. The decoding process takes out the 3D coordinate data of the corresponding points by the index and calculates the plane equation corresponding to each group of data as the first generation of population taking. The plane equation is expressed as equation (2).

$$z = ax + by + c. \tag{2}$$

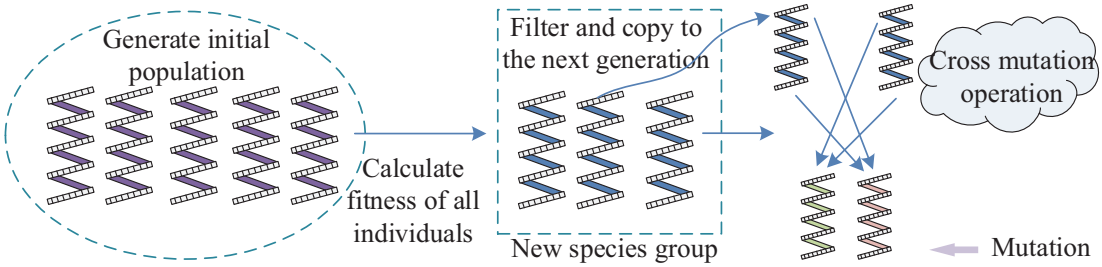


**Fig. 2.** Schematic diagram of genetic algorithm principle.

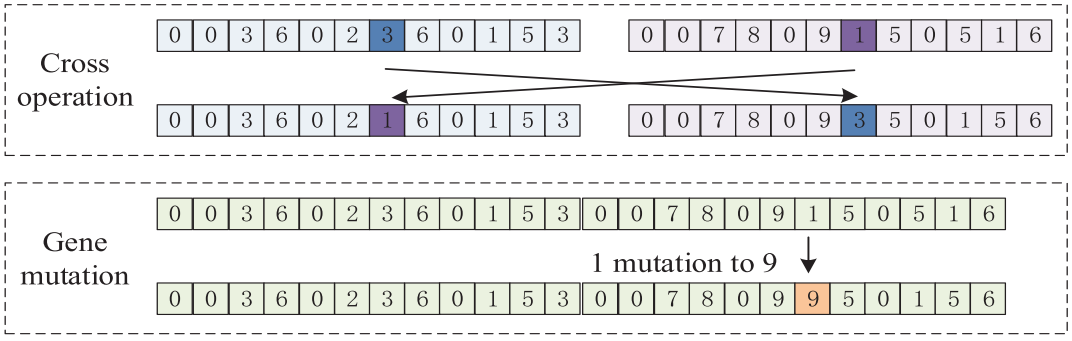


**Fig. 3.** Schematic diagram of gene crossover and mutation.

Because the effective focal range for non-ferrous laser marking is ±1.5 mm, the study sets it as the threshold $t$ of the RANSAC algorithm. Then the distances from all points in the point cloud data residual set to each plane were calculated. The distances are calculated as in equation (3).

$$d_i = |ax_i + by_i + c - z_i| / \sqrt{a^2 + b^2 + 1}. \tag{3}$$

In equation (3), $c,b,c$ are all plane equation coefficients. The individual fitness is calculated as in equation (4).

$$w_k = S + 3/N. \tag{4}$$

In equation (4), $S$ is the amount of points within each plane and $N$ is the sum of points. Replication of the new population was performed according to the index chromosome fitness. The sum of fitness values for this population is calculated as in equation (5).

$$F = \sum_{k=1}^{10} w_k. \tag{5}$$

After the sum of fitness is obtained by equation (5), the probability of each chromosome being replicated needs to be calculated as in equation (6).

$$P_k = \frac{w_k}{F}. \tag{6}$$

The study is based on the roulette wheel selection method, where the roulette wheel is rotated 10 times and the index chromosome of a new population is selected each time. The implementation of the roulette wheel selection method in the program is based on generating [0,1] pseudo-random numbers for selection. It ends until 10 new populations are selected. After the population replication is performed, the populations are crossed. The number of index chromosomes crossed is equal to the total number of index chromosomes multiplied by the crossover probability. The study set the crossover probability value to 0.2. The two individual spreads, the crossover chromosome objects were also determined as 10 random numbers obtained in the range of 0 to 1. Two of the individual chromosomes below the crossover probability underwent crossover variation. In addition to crossover, mutations in the population are also genetic mutations. The study set the mutation probability to 0.01. The principle of gene mutation and gene crossover is illustrated in Figure 3.

After the mutation operation, the population completes the first generation process and iterates further, and the plane equation with the most internal points at the completion of the max iterations or when the desired value is reached is the final target equation. Based on the above content, GA algorithm is used to optimize the random sampling process of RANSAC algorithm, and thus an improved RANSAC algorithm is obtained. After the improvement, it is applied to the fitting of planar equations on the graded surfaces. The specific improvement process is as follows: First, the original point cloud data is preprocessed to remove obvious noise and outliers to ensure the quality of the data. Then, GA algorithm is used to generate the initial population of the pre-processed data, and each individual in the population represents a set of possible plane equation parameters. Each individual is evaluated by the fitness function, which mainly considers the number of points in the plane equation and the fitting error. After several iterations, when the algorithm converges or reaches the preset maximum number of

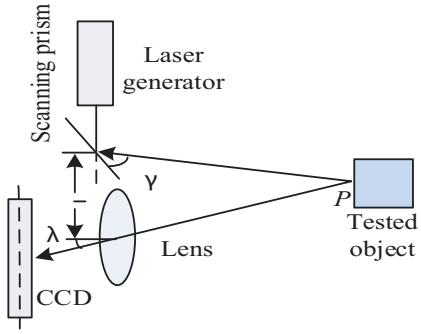


**Fig. 4.** Measurement principle of 3D line laser scanner.

iterations, the individual with the highest fitness is selected as the parameter of the final plane equation. At this time, the plane equation obtained not only has high fitting precision, but also has strong robustness, and can effectively resist the influence of noise. Finally, the optimized plane equation is applied to the laser marking process of non-ferrous metal ingot, and the position of the laser marking lens is automatically adjusted by calculating the rotation Angle or displacement, so as to ensure that the marking content is clear and complete.

### 3.2 Non-contact casting ingot laser marking method to achieve

There are two common alignment systems: a single-point rangefinder-based alignment system and a 3D line-laser scanner-based alignment system. The study of metal casting ingot marking requires accurate acquisition of the casting ingot plane equation and normal vector, and the use of mechanical structures for alignment. Therefore, the 3D line laser scanner based alignment system is chosen to obtain the plane information of the casting ingot surface and to achieve automatic alignment and vertical focusing. The measurement principle of the 3D line laser scanner is shown in Figure 4.

The measurement coordinate system is established with the laser reflecting at the scanning prism as the origin, and the three-dimensional coordinates are expressed as in equation (7).

$$\begin{cases} X = \dfrac{\sin\gamma\sin\lambda\sin\omega}{\sin(\gamma+\lambda)}L \\ Y = \dfrac{\cos\gamma\sin\omega}{\sin(\gamma+\lambda)}L \\ Z = \dfrac{\sin\gamma\sin\lambda\cos\omega}{\sin(\gamma+\lambda)}L \end{cases}. \tag{7}$$

In equation (7), $\omega$ is the angle acquired by the 3D line laser scanner according to the sensor, $\gamma$ and $\lambda$ are the emission angle and incident angle of the laser light respectively, and $L$ is the baseline length. The non-ferrous casting ingot point cloud data is acquired by a 3D line laser scanner that sweeps steadily over the surface of the non-ferrous casting ingot driven by a servo motor at an even speed. The digital alignment function is accomplished by coordinated rotation of the horizontal-$X$ and $Y$ axes of the pendulum. The measurement coordinate system of the 3D line laser scanner and the pendulum table coordinate system of the pendulum table do not coincide. The 3D point-cloud data measured by the system needs to be transformed into the pendulum table coordinate system by translation and rotation between the coordinate systems. Any transformation between coordinate systems can be decomposed into translation transformation and rotation transformation between coordinate systems. The transformation method is as in equation (8).

$$\begin{bmatrix} {}^{B}P \\ 1 \end{bmatrix} = \begin{bmatrix} {}^{A}_{B}R & {}^{A}P_{BORG} \\ 0\ \ 0 & 0\ \ 1 \end{bmatrix} \begin{bmatrix} {}^{A}P \\ 1 \end{bmatrix}. \tag{8}$$

In equation (8), ${}^{A}_{B}R$ is the $3\times3$ rotation matrix of $\{B\}$ with respect to that system $\{A\}$, ${}^{A}P_{BORG}$ is the $3\times1$position vector matrix of the origin of $\{B\}$ with respect to $\{A\}$. ${}^{A}$P and ${}^{B}$P are the 3D coordinates of the point-$P$ in the two coordinates, and the $4\times4$ matrix $T$ in the equation is the chi-square transformation matrix. In the non-contact automatic alignment mechanism, the 3D line laser scanner is installed next to the laser marking lens. The position between the measurement and the pendulum coordinate system is relatively fixed to reduce the alignment time, taking into account the complexity of the coordinate system transformation. After the point-cloud data is transformed between the coordinate systems, all data values are transformed, and the point cloud data is then ready for plane fitting. The previous study has performed a 3D plane fitting using the improved RANSAC algorithm. On the ground of the fitted plane equation, the plane's normal vector is found, and then the angle between the coordinate axis and the normal vector is determined. The clip angle is calculated as in equation (9).

$$\begin{cases} \alpha = ar\cos\dfrac{a}{\sqrt{a^2+c^2}} \\ \beta = ar\cos\dfrac{b}{\sqrt{a^2+b^2+c^2}} \\ \gamma = ar\cos\dfrac{c}{\sqrt{a^2+c^2}} \end{cases}. \tag{9}$$

In equation (9), $(a,b,c)$ is the normal vector obtained after plane fitting, and $\alpha$, $\beta$, $\gamma$ are the angle among the $X$, $Y$, $Z$ axes. The effect of the angle is shown in Figure 5.

After the rotation $\alpha$ and $\beta$ angles of the $X$ and $Y$ of the pendulum, the laser marking lens will be in a staggered parallel state with the surface of the object to be measured. The next step is to determine the marking position and vertical focus according to the actual situation and geometric relationship. In the initial state, the center of the 3D line laser scanner and the center of the laser marking lens are mounted on the same horizontal line, and the center of the lens of both is on the same line with the center line of the measured plane of the casting ingot, with the pendulum coordinate system as the current coordinate system. To make the laser marking lens face parallel to the marking surface, the distance traveled by the pendulum along the $X$ and $Y$ in the righting rotation is recorded, and the reverse motion of the base coordinate system is used so

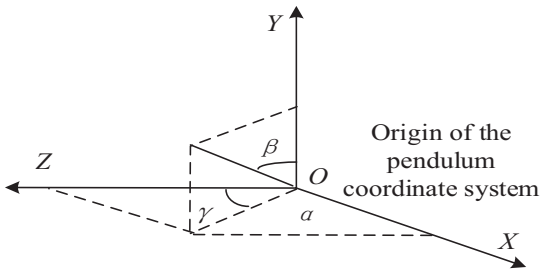


**Fig. 5.** Effect of angle between normal vector and normal vector.

that the laser beam of the 3D laser scanner and the laser marking lens can be projected onto the surface of the casting ingot. When the pendulum table rotates around its $X$ axis, the distance traveled by the base $Y$ axis is calculated as in equation (10).

$$\begin{aligned} a &= [(L_1 + L_2 + L_3) \times \sin\alpha] \div \cos\alpha \\ &= \left\{ \left[ L_1 + L_2 + \frac{(1-\cos\alpha)}{\sin\alpha} \times d \right] \times \sin\alpha \right\} \div \cos\alpha . \end{aligned} \quad (10)$$

In the formula (10), $L_1$ is the distance from the center of the laser marking head to the casting spindle before rotation, $L_2$ is the distance from the lens center to the pendulum coordinate system $Y$ axis in the $Z$ axis direction, $L_3$ is the distance between the intersection point of the lens center and the pendulum coordinate system $Y$ in the $Z$ direction before and after rotation. $d$ is the distance from the origin of the pendulum coordinate system to the lens center in the $Y$ axis direction. Similarly, when the pendulum table rotates around its axis, the distance of the base $X$ axis movement can be calculated. The positive view of the pendulum table in both cases is shown in Figure 6.

The laser marking lens is perpendicular to the marked surface, and the laser beam of the laser marking lens can be projected onto the marked surface, while the scan line of the line laser scanner is on the surface of the casting ingot. The three servo motors decomposed in the base coordinate system move the distance as in equation (11).

$$\begin{cases} x' = d\cos\beta\cos\alpha \\ y' = d\sin\beta \\ z' = d\cos\beta\sin\alpha \end{cases} . \quad (11)$$

In equation (11), $x'$, $y'$, $z'$ is the distance traveled by the three servo motors of the base, $\alpha$, and $\beta$ is the rotation angle of the pendulum around the coordinate system $X, Y$ axis. After the three servo motors complete the distance traveled, the signal is transmitted to the laser marker to start marking. Combining the above operations, the study uses the GA algorithm to perform bootstrap sampling of the RANSAC algorithm based on probabilities, and combines the two for simulation, thereby optimizing the shortcomings of the RANSAC algorithm for random sampling. According to the plane equation fitted by the improved RANSAC algorithm, the plane's normal vector is found, and the angle between the coordinate axis and the normal vector is determined by the normal vector, so that the automatic alignment and vertical focusing functions are realized. Finally, the position of the marker is determined according to the actual situation by using the set relationship to realize the motion control of the mechanical function.

## 4 Performance analysis of laser marking method for metal casting ingots based on GA-RANSAC algorithm

Due to the random sampling characteristic of the RANSAC algorithm, the algorithm requires a large increase in the number of extractions if better plane equations are to be obtained when plane fitting is performed, but this is not very efficient for training. For this reason the study uses the GA algorithm to optimize it. To test the optimization effect of the algorithm, the study compares the training of RANSAC algorithm before and after the improvement in the same environment. Also to further test the convergence performance of the algorithm, several popular plane fitting methods are added for comparison. Specifically, the plane fitting method built on least squares, improved particle swarm algorithm and priori error decomposition are Algorithm 1–3, respectively. The specific training situation is shown in Figure 7.

In Figure 7, with the increasing number of iterations, the percentage of interior points in the plane gradually increases. The improved GA-RANSAC algorithm has the fastest iteration speed and the largest curve change. Algorithm 1 and Algorithm 2 have not reached the target value by 8000 iterations; Algorithm 3 has reached the target value by 3716 iterations, which is 1893 iterations more than the GA-RANSAC algorithm. This is because the introduction of GA algorithm makes the selection of initial interior points more reasonable and avoids the blindness of random selection in traditional RANSAC algorithm. In addition, the optimization mechanism of GA algorithm makes each iteration closer to the optimal solution, thus speeding up the convergence process. The RANSAC optimized with GA algorithm has better convergence and can reach the training learning goal faster.

To further verify the improved algorithm is more efficient than the traditional RANSAC algorithm. The research was programmed and simulated under MATLAB software. First, Lloyd's line laser scanner was used to obtain surface point cloud data of aluminum and copper ingot, and then the key parameters of the two were compared, as shown in Table 1.

In the Table above, the average iterations of the RANSAC is 1821, the ratio of internal points is 0.951, and the iteration time is 7.467 s. It can be seen that at the same point cloud data points, the parameters in the two algorithms will be able to change in a small way, but in the iterations and calculation time, the GA-RANSAC is significantly reduced. It is more accurate and efficient than the other four calculations.

To test the noise reduction effect of the algorithm, a study was conducted to find the laser markings using the algorithm under different signal-to-noise ratios, and the fitting accuracy of the markings before and after using the algorithm was compared and recorded in Figure 8.

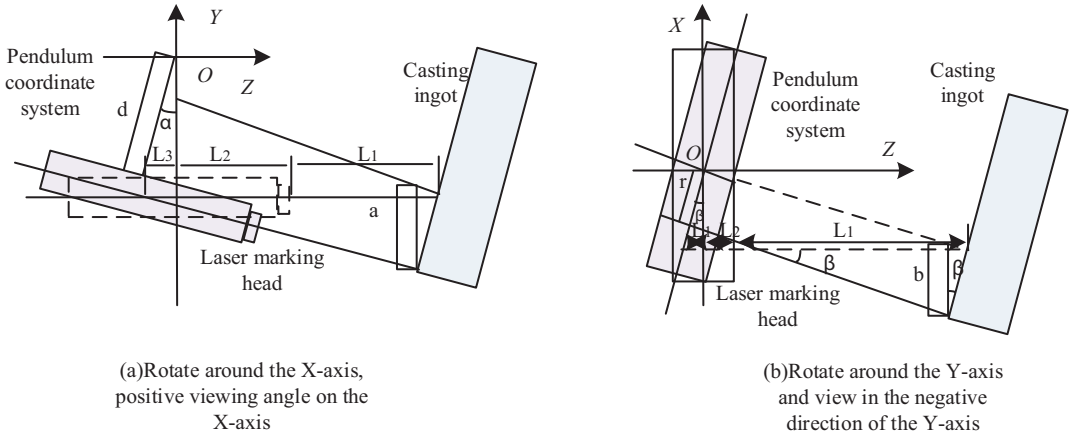


(a)Rotate around the X-axis, positive viewing angle on the X-axis

(b)Rotate around the Y-axis and view in the negative direction of the Y-axis

**Fig. 6.** Views of the corresponding directions of the swing table in 2-scenarios.

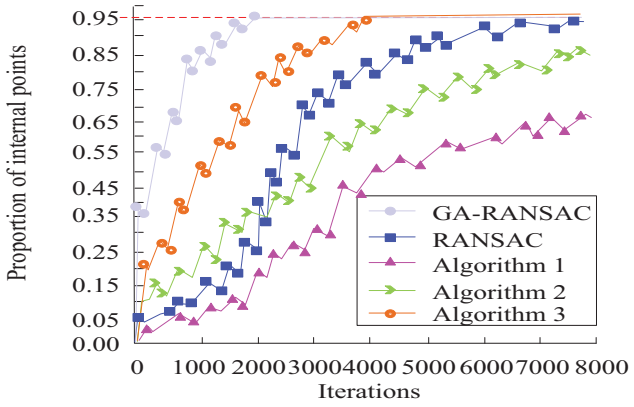


**Fig. 7.** Comparison of Training Conditions of Different Plane Fitting Methods.

In Figure 8, with the increasing noise, the marking accuracy of both methods has a decreasing trend. The change of the marking accuracy curve of laser marking after using the algorithm is relatively gentle, and the marking accuracy is 98.47% when the noise ratio is 0.1, and 96.98% when the noise ratio is 1.0, which is only 1.49% lower; the change of the traditional mechanical marking method is larger. When the noise ratio is 0.1, the marking accuracy is 92.48%, and when the noise ratio is 1.0, the marking accuracy is 83.76%, which is a decrease of 8.72%. The comprehensive content in Figure 8 shows that the GA-RANSAC can availably remove the noisy outer point and enhance the accuracy of laser marking.

To further test the denoising effect of the algorithm, the study was conducted and simulated using the research design algorithm for plane fitting of metal ingot plane data at noise ratios of 0.35 and 0.75, respectively. The scaling error of the algorithm was obtained as shown in Figure 9.

In Figure 9, at a noise ratio of 0.35, the marking error value of the laser marking method designed by the research mainly fluctuates between 0.002 and 0.020 mm. The least value of error is 0.0018 mm and the max is 0.026; when the noise ratio is 0.75, the marking error mainly fluctuates between 0.005 and 0.025 mm, the least value of error is 0.038 and the max is 0.025 mm. Combining the contents in Figures 9a and 9b, the mean relative error value of the research design laser marking method is 0.012 mm. It meets the production requirements.

The stability of the laser marking method (Method 1) designed for the study was not tested. The experiments were performed in the same experimental environment using Method 1 and the more popular laser marking methods for laser marking simulations with different data sizes. The comparison methods are laser marking based on integrated network (method 2), laser online tracking marking considering the target motion state (method 3), laser flying marking based on DSP and CPLD (method 4), and laser marking control based on embedded network (method 5). And the variation of marking accuracy is recorded in Figure 10.

In Figure 10, with the increase of the number of engraved samples, the curve of engraving accuracy of each method showed a decreasing trend. The average marking accuracy of method 1 is 98.02%, which decreases by 2.13% when the sum of samples arises from 250 to 2400; the average marking accuracy of method 2 decreases by 18.34%, which is 16.21% more than that of method 1; the average marking accuracy of method 3 decreases by 10.05%, which is 7.92% more than that of method 1; the average marking accuracy of method 4 decreases by 12.66%, which is 10.53% more than that of method 1; the average marking The average marking accuracy of method 4 decreased by 12.66%, 10.53% more than that of method 1; the average marking accuracy of method 5 decreased by 22.78%, 20.65% more than that of method 1. A comprehensive analysis of Figure 10 shows that method 1 is more accurate and stable than the other four methods.

To further validate the performance of the method, the study introduced F1 value, accuracy, root mean square error (RMSE), and running time as evaluation metrics for the performance of the method. The same batch of aluminum ingot material was used for laser marking in two experiments and the corresponding index values were recorded in Table 2.

In Table 2, the average F1 value of method 1 is 96.42, the average accuracy is 98.24%, the RMSE is 0.236, and the running time is 18.40 s. The other four methods have lower values than method 1 except for the running time and

**Table 1.** Surface fitting parameter results.

| Project | Copper ingot | | | Aluminum ingot | | |
|---|---|---|---|---|---|---|
| | Iterations | Inner point ratio | Iteration time(s) | Iterations | Inner point ratio | Iteration time(s) |
| RANSAC | 7248 | 0.952 | 51.892 | 7189 | 0.950 | 51.565 |
| GA-RANSAC | 1816 | 0.967 | 7.423 | 1825 | 0.968 | 7.511 |
| Algorithm 1 | 25012 | 0.950 | 100.924 | 25001 | 0.952 | 101.352 |
| Algorithm 2 | 20312 | 0.949 | 82.133 | 20043 | 0.951 | 83.461 |
| Algorithm 3 | 3821 | 0.953 | 21.463 | 3825 | 0.954 | 21.472 |

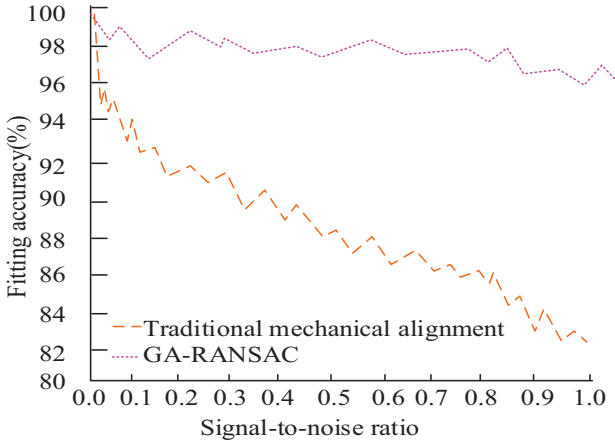


**Fig. 8.** Changes in the curve of laser marking affected by noise before and after using the RANSAC algorithm.

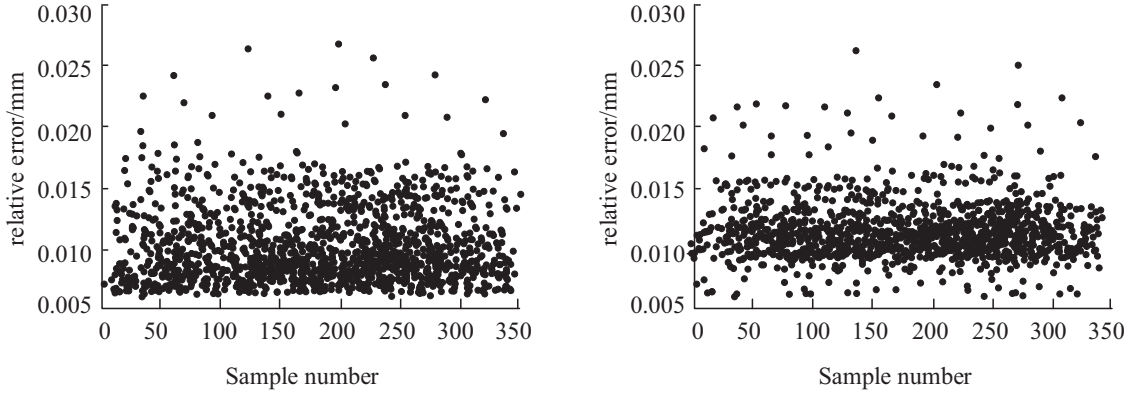


**Fig. 9.** Scatter distribution of errors in laser marking algorithms designed by the research institute under different noise ratios.

RMSE, and the running time and error are greater than method 1. A comprehensive analysis of the contents in Table 2 shows that method 1 can efficiently and accurately laser mark the metal casting ingots and improve the production efficiency. By comparing the data in Table 2 and Figure 10, it is found that the F1 value and accuracy rate of method 1 are close to the optimal value, indicating that it can effectively reduce mismarking and missing targets in the marking process. The RMSE value of method 1 is low, indicating that the error of the marking position is small and the marking precision is high. In addition, the stability and robustness of method 1 are further verified by comparing the variation of marking accuracy under different data scales. Based on the above content, the research evaluates its accuracy in multiple directions and angles.

In order to verify the practical application effect of the laser marking method proposed in the study, a designed target drawing was used to carry out laser marking with the research design method. The marking results are shown in Figure 11.

As shown in Figure 11, the surface pattern of copper ingot has high clarity and clear texture, which is basically consistent with the design target drawing. In addition, through the microscopic observation of the marking area, it is found that the edge of the laser beam on the surface of the

**Table 2.** Comparison of evaluation indicator data for various methods.

| Project | | M1 | M2 | M3 | M4 | M5 |
|---|---|---|---|---|---|---|
| Test 1 | F1 | 96.42 | 82.34 | 92.54 | 88.16 | 76.34 |
| | Accuracy (%) | 98.23 | 84.26 | 93.23 | 89.37 | 78.12 |
| | RMSE | 0.235 | 0.751 | 0.418 | 0.668 | 0.879 |
| | Time(s) | 18.41 | 47.56 | 25.12 | 33.94 | 59.45 |
| Test 2 | F1 | 96.43 | 82.33 | 92.38 | 88.12 | 76.34 |
| | Accuracy (%) | 98.25 | 84.96 | 93.24 | 89.42 | 78.11 |
| | RMSE | 0.236 | 0.752 | 0.425 | 0.667 | 0.880 |
| | Time(s) | 18.39 | 47.48 | 25.68 | 34.02 | 60.01 |

Note: *M1: Method 1.

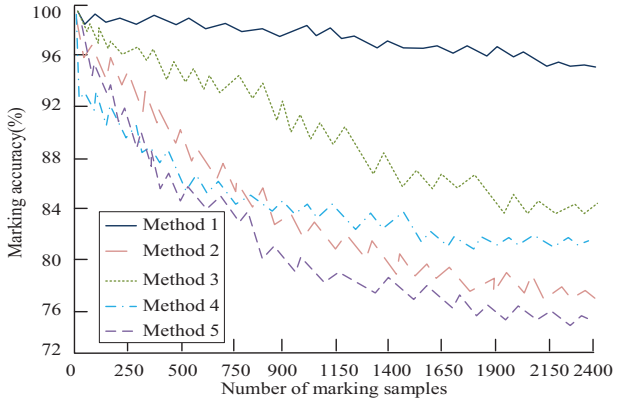


**Fig. 10.** Variation Curve of Marking Accuracy for Different Data Scales and Methods.

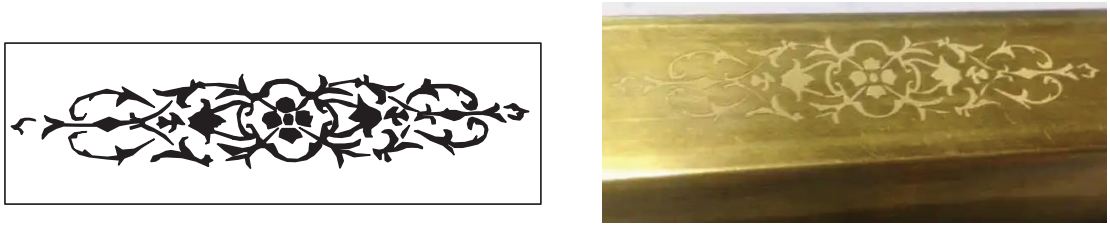

(a) Design object drawing (b) Marking result

**Fig. 11.** The practical application effect of the designed laser marking method for non-ferrous metals is studied.

copper ingot is orderly, and there is no obvious heat-affected zone, which indicates that the method can effectively control the thermal damage while ensuring the marking accuracy. Compared with conventional marking methods, the laser marking method based on GA-RANSAC algorithm presented in this study shows significant advantages in detail processing and heat effect control. Specifically, the method ensures high precision and clarity of the marking pattern by optimizing the focusing and scanning path of the laser beam.

## 5 Conclusion

When laser marking the surface of a non-ferrous casting ingot, the laser marking lens must be able to maintain precise vertical focus on the surface of the casting ingot. For this purpose, the GA-RANSAC algorithm is used to fit the equation to the plane of the metal casting ingot to find the closest plane and remove the noise from the surface of the ingot itself. Digital correction is performed based on the fitted plane equations to improve the marking accuracy. Thus, a laser marking method for non-ferrous casting ingots based on the improved RANSAC algorithm is designed. Through experimental analysis, the GA-RANSAC algorithm iterates up to 1823 times to reach the target inner point occupancy value of 0.95, which has good convergence. Under different noise ratios, the average relative error value of the laser marking method is 0.012 mm, which meets the production requirements. The average marking accuracy of the method is 98.02% as the number of marked samples increases, and the marking accuracy decreases by 2.13% during the process of increasing the

number of samples from 250 to 2400, which can be concluded that the method has good stability. The F1 value represents the combined performance of the model's accuracy and recall rate when dealing with the marking task. The average F1 value of this method is 96.42, the average accuracy is 98.24%, the RMSE is 0.2.236, and the running time is 18.40 s. It can efficiently and accurately laser mark the metal casting ingots and improve the production efficiency. In the subsequent research process, we can consider the corresponding marking requirements of different metal casting ingots and design a more flexible marking mechanical structure.

## Funding

No.

## Conflicts of interest

The author declares that the paper has no conflicts of interest and the author has full control of all primary data and that the author agrees to allow the journal to review data if requested.

## Data availability statement

All data generated or analysed during this study are included in this published article.

## Author contribution statement

All contributions to the article belong to Rui Zheng.

## References

1. D.A. Konchus, E.I. Pryakhin, A.V. Sivenkov, Structural variations on the surface of metallic products at laser marking, CIS Iron Steel Rev. **22** (2021) 96–101
2. X. Shu, J. Ding, The study on laser marking glass fiber material, Grand Altai Res. Educ. **1** (2020) 111–118
3. J. Wei, F. Ning, C. Bai, T. Zhang, G. Lu, H. Wang, X. Zhou, An ultra-thin, flexible, low-cost and scalable gas diffusion layer composed of carbon nanotubes for high-performance fuel cells, J. Mater. Chem. A **8** (2020) 5986–5994
4. L. Huang, S. Xu, Z. Wang, K. Xue, J. Su, Y. Song, R. Ye, Self-reporting and photothermally enhanced rapid bacterial killing on a laser-induced graphene mask, ACS Nano **14** (2020) 12045–12053
5. S. Canaz Sevgen, F. Karsli, An improved RANSAC algorithm for extracting roof planes from airborne lidar data, Photogrammetr. Record **35** (2020) 40–57
6. Z. Li, B. Zhang, K. Li, T. Zhang, X. Yang, A wide linearity range and high sensitivity flexible pressure sensor with hierarchical microstructures via laser marking, J. Mater. Chem. C **8** (2020) 3088–3096
7. M. Pandey, B. Doloi, B. Bhattacharyya, Parametric study on laser marking of circular shape on stainless steel 304, Int. J. Precision Technol. **10** (2021) 3–22
8. A. Korakana, S. Korakana, N. Ulmek, A.K. Pagare, Analyzing the effect of the parameters of laser etching process influencing the corrosion resistance and surface roughness of marine grade 316 stainless steel, Mater. Today: Proc. **32** (2020) 452–462
9. N.G. Rasskazchikov, A.A. Polyakova, Researching of laser marking process and its optimization, Russ. Internet J. Ind. Eng. **7** (2020) 9–13
10. S. Cucerca, P. Didyk, H.P. Seidel, V. Babaei, Computational image marking on metals via laser induced heating, ACM Trans. Graphics **39** (2020) 1–70
11. F. Eyahanyo, T. Rath, Investigations on the effects of low laser infrared marking energy and barcode size on 2D data matrix code detection on apples, Appl. Eng. Agric. **36** (2020) 829–838
12. M. Drobnitzky, A. Vom Endt, A. Dewdney, A phantom based laser marking workflow to visually assess geometric image distortion in magnetic resonance guided radiotherapy, Phys. Imag. Radiat. Oncol. **17** (2021) 95–99
13. F. Gönültas, M.E. Atik, Z. Duran, Extraction of roof planes from different point clouds using RANSAC algorithm, Int. J. Environ. Geoinform. **7** (2020) 165–171
14. R. Cao, Y. Wang, Y. Zhang, J. Mao, Optimal time selection for ISAR imaging of ship target via novel approach of centerline extraction with RANSAC algorithm, IEEE J. Selected Topics Appl. Earth Observ. Remote Sens. **15** (2022) 9987–10005
15. J. Bai, D. Qin, L. Ma, M.B. Teklu, An improved RANSAC algorithm based on adaptive threshold for indoor positioning, Mobile Inform. Syst. **2021** (2021) 1–14
16. Z. Hossein-Nejad, M. Nasri, Natural image mosaicing based on redundant key point elimination method in SIFT algorithm and adaptive RANSAC method, Signal Data Process. **18** (2021) 147–162
17. S. Zhang, S. Li, B. Zhang, M. Peng, Integration of optimal spatial distributed tie-points in RANSAC-based image registration, Eur. J. Remote Sens. **53** (2020) 67–80
18. A. Singh, S.K.P. Kushwaha, S. Nandy, H. Padalia, An approach for tree volume estimation using RANSAC and RHT algorithms from TLS dataset, Appl. Geomat. **14** (2022) 785–794
19. J. Li, Q. Hu, M. Ai, Point cloud registration based on one-point Ransac and scale-annealing biweight estimation, IEEE Trans. Geosci. Remote Sens. **59** (2021) 9716–9729
20. S. Afsal, A. Linsely, Optimal process of video stabilization using hybrid RANSAC-MSAC algorithm, Int. J. Intell. Syst. Appl. Eng. **11** (2023) 564–571

**Cite this article as**: Rui Zheng, Laser marking method for nonferrous metal casting ingots based on improved RANSAC algorithm, Manufacturing Rev. **12**, 7 (2025), https://doi.org/10.1051/mfreview/2025002